Assessing the impact of the Electron-Ion Collider in China on deeply virtual Compton scattering*

Yuan-Yuan Huang (黄源源)[1,2] Xu Cao (曹须)[2,3†] Taifu Feng (冯太傅)[1‡] Krešimir Kumerički[4§] Yu Lu (陆宇)[3¶]

[1]Department of Physics, Hebei University, Baoding 071002, China
[2]State Key Laboratory of Heavy Ion Science and Technology, Institute of Modern Physics, Chinese Academy of Sciences, Lanzhou 730000, China
[3]University of Chinese Academy of Sciences, Beijing 100049, China
[4]Department of Physics, University of Zagreb Faculty of Science, HR-10000 Zagreb, Croatia

Abstract: We assess the impact of measuring deeply virtual Compton scattering (DVCS) off protons using the planned detector at the Electron-Ion Collider in China (EicC), which is proposed as an upgrade to the High Intensity Heavy-Ion Accelerator Facility (HIAF). We develop a neural-network architecture to flexibly parameterize Compton form factors (CFFs), reliably extrapolate into unmeasured kinematic regions, and provide robust uncertainty estimates using the replica method. The framework is fitted to available worldwide DVCS data using the `Gepard` software. We find a significant reduction in the uncertainties of all CFFs after incorporating pseudo-data from single and double polarization asymmetries at the EicC, with particularly strong improvements in the sea-quark region.

Keywords: deeply virtual Compton scattering, neural network, electron ion collider, Compton form factors

DOI: 10.1088/1674-1137/ae457e **CSTR:** 32044.14.ChinesePhysicsC.50053110

I. INTRODUCTION

The three-dimensional distributions of quarks and gluons inside hadrons, encoded in terms of generalized parton distributions (GPDs), can be probed via hard exclusive processes [1−4]. Among these, the cleanest channel is deeply virtual Compton scattering (DVCS) [5−9], which is a central physics objective of future electron-ion colliders, where it will be explored across complementary kinematic regions with polarized beams.

The electron-ion collider (EIC) at Brookhaven National Laboratory (BNL) provides a high-precision experimental platform for studying gluons in nucleons and nuclei [10, 11]. Fixed-target experiments at Jefferson Lab (JLab), together with its potential upgrade [12], investigate the valence-quark region and the onset of sea-quark contributions in great detail. Strategically designed to complement the EIC and JLab programs, the Electron-Ion Collider in China (EicC) aims to survey the sea-quark regime with unprecedented precision [13−15]. Alongside these efforts, the planned Large Hadron-Electron Collider (LHeC) at CERN would extend coverage deep into the small-x domain [16, 17]. Together, these facilities form a global program spanning a remarkably broad kinematic range. Such coverage will make it possible to reconstruct GPDs with controlled systematic uncertainties, leading to a more precise understanding of nucleon tomography [18−21], spin structure [7], and mechanical properties [22], which are aspects of the nucleon's internal structure that remain insufficiently understood.

Although DVCS (and other exclusive processes involving GPDs) is sensitive to GPDs, it does not probe them directly. Instead, GPDs enter observables through Compton form factors (CFFs), which are integrals of the GPDs weighted by a hard-scattering kernel that is calculable order by order in perturbative QCD. Therefore, extracting the GPDs themselves requires deconvoluting this highly nontrivial relation, a challenge associated with the

Received 23 December 2025; Accepted 11 February 2026; Accepted manuscript online 12 February 2026

* Supported by the National Key R&D Program of China (2023YFA1606703), the National Natural Science Foundation of China (12547111, 12235008, 12405105) and (PK.1.1.10.0004) co-financed by the European Union and through the European Regional Development Fund - Competitiveness and Cohesion Programme 2021-2027. TF also thanks the Hebei Natural Science Foundation (A2022201017, A2023201041) and Natural Science Foundation of Guangxi Autonomous Region (2022GXNSFDA035068)

† E-mail: caoxu@impcas.ac.cn
‡ E-mail: fengtf@hbu.edu.cn
§ E-mail: kkumer@phy.hr
¶ E-mail: ylu@ucas.ac.cn

issue of "shadow GPDs" [23, 24]. The extraction and separation of individual CFFs from data are greatly facilitated by measured angular distributions and spin asymmetries and constitute the first step toward determining GPDs from their associated form factors. After several early attempts at local CFF extraction from single kinematic points [25–27], global fits to the available data from JLab Hall A, CLAS, COMPASS, and HERMES collaborations have provided quantitative information on leading-twist chiral-even CFFs. This procedure is inherently complex owing to the large number of unknown functions and the multiple independent kinematic variables on which they depend. Non-parametric neural networks (NNs) [28], Gaussian process regression [29], and other flexible parameterization methods [30, 31] have proved useful for one- and two-dimensional problems, such as standard parton distribution functions (PDFs). To minimize model dependencies and uncertainties arising from extrapolation and interpolation in multidimensional kinematic space, NN parameterizations of CFFs offer the unique advantage of flexibility and hyperparameter choice [32–34]. Such parameterizations have enabled progress in the extraction of gravitational form factors from DVCS data [35] and in the flavor separation of key CFFs [36, 37].

Several categories of GPD models have been proposed, including the double distribution ansatz [38], representations in the conformal-moment space [39], string-inspired parameterization in AdS space [40], basis light-front quantization [41], and NN approaches [42, 43]. Some of these have already been used in global fits to DVCS data [44–49]. However, systematic uncertainties owing to model rigidity are not fully understood. Upcoming efforts, aided by lattice-QCD calculations of GPDs [50, 50–54], within either the large-momentum effective theory [55, 56] or the pseudo-distribution approach [57], are expected to yield more reliable uncertainty estimates.

Currently, the impact of new or proposed DVCS experiments on CFF extractions can be efficiently quantified using suitable NN architectures with the Monte Carlo (MC) replica method, possibly alongside the Bayesian reweighting procedure [33]. The relevance of the transversely polarized proton beam-spin asymmetries at the EicC and their sensitivity to the corresponding dominant CFF have been demonstrated in Ref. [15] using such an approach. For this purpose, the pseudo-data of DVCS measurements at the EicC were generated without considering the detector efficiency [58]. In this study, we extend these previous investigations by incorporating realistic detector coverage and efficiency and by generating all measurable spin asymmetries. Subsequently, NN parameterizations of CFFs are used to assess the impact of future EicC DVCS measurements on determining all leading-order CFFs. Our analysis framework is constructed on `Gepard`, a Python software package for the study of GPDs [44, 47].

II. SIMULATION OF DVCS AND EXTRACTION OF CFFS

The exclusive photon electroproduction process $ep \to e'p'\gamma$ is the coherent sum of the electromagnetic Bethe-Heitler (BH) and DVCS amplitudes, facilitating access to GPDs, as shown in Fig. 1. At leading twist, the quark-helicity-conserving GPDs H, E, $\widetilde{H}$, and $\widetilde{E}$ contribute to DVCS through the corresponding CFFs $\mathcal{H}$, $\mathcal{E}$, $\widetilde{\mathcal{H}}$, and $\widetilde{\mathcal{E}}$. The five-fold differential cross section is

$$\begin{aligned} \mathrm{d}\sigma(\phi,\phi_S) \equiv \frac{\mathrm{d}\sigma^{ep\to e'p'\gamma}}{\mathrm{d}x_B\mathrm{d}Q^2\mathrm{d}|t|\mathrm{d}\phi\mathrm{d}\phi_S} = \mathrm{d}\sigma_{\mathrm{UU}}[1 + h_l A_{\mathrm{LU}} + h_p A_{\mathrm{UL}} \\ + h_l h_p A_{\mathrm{LL}} + S_{\mathrm{T}}(A_{\mathrm{UT}} + h_l A_{\mathrm{LT}})], \end{aligned} \tag{1}$$

where $h_l/2$ ($h_p/2$) is the electron (proton) beam helicity, and S_{T} is the component of the incoming proton spin that is transverse to the virtual photon direction. The kinematic variables are explained in the caption of Fig. 1, and at leading twist, the skewness ξ is related to Bjorken-x via $\xi = x_B/(2-x_B)$. Here, ϕ is the azimuthal angle between the lepton and real-photon production planes [59]. The angle ϕ_S denotes the azimuthal orientation of the trans-

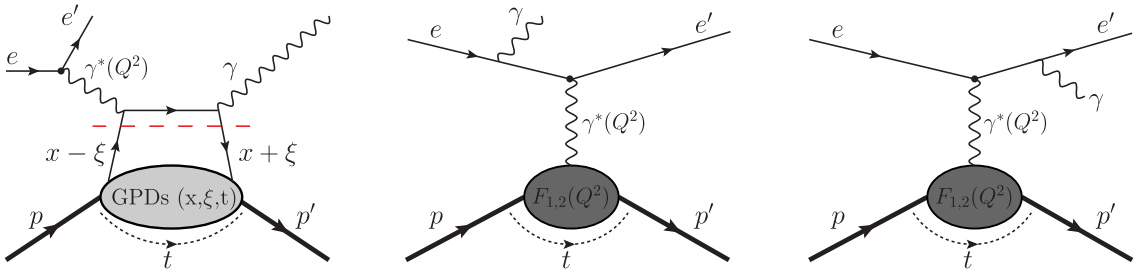

Fig. 1. (color online) Deeply virtual Compton scattering (left) and the accompanying Bethe-Heitler process (middle and right). $Q^2 = -q^2$ is the negative four-momentum squared of the virtual photon. Other kinematic variables are as follows: x is the average longitudinal momentum fraction of the active quark, ξ is the half longitudinal momentum fraction transferred to the nucleon, and t is the squared four-momentum transferred to the nucleon. $F_{1,2}$ are elastic form factors in the Dirac-Pauli representation.

verse proton-spin component with respect to the lepton scattering plane. Integrating over ϕ_S reduces the cross section $\mathrm{d}\sigma(\phi,\phi_S)$ to the four-fold counterpart $\mathrm{d}\sigma(\phi) \equiv \mathrm{d}\sigma^{ep\to e'p'\gamma}/\mathrm{d}x_B\mathrm{d}Q^2\mathrm{d}|t|\mathrm{d}\phi$, in which the $\cos\phi$ modulation of the BH-DVCS interference term is sensitive to the real part of the CFFs $\mathcal{H}$ in the case of proton DVCS:

$$\sigma_{\mathrm{UU},I}^{\cos\phi} \propto \mathrm{Re}\left[F_1\mathcal{H} + \xi(F_1+F_2)\widetilde{\mathcal{H}} - \frac{t}{4M^2}F_2\mathcal{E}\right]. \tag{2}$$

The longitudinally polarized proton or electron beam single-spin asymmetries are defined as

$$A_{\mathrm{LU}} = \frac{\mathrm{d}\sigma(\phi)^{\rightarrow} - \mathrm{d}\sigma(\phi)^{\leftarrow}}{\mathrm{d}\sigma(\phi)^{\rightarrow} + \mathrm{d}\sigma(\phi)^{\leftarrow}}, \quad A_{\mathrm{UL}} = \frac{\mathrm{d}\sigma(\phi)^{\Rightarrow} - \mathrm{d}\sigma(\phi)^{\Leftarrow}}{\mathrm{d}\sigma(\phi)^{\Rightarrow} + \mathrm{d}\sigma(\phi)^{\Leftarrow}}, \tag{3}$$

where the arrows $\rightarrow$ ($\leftarrow$) or $\Rightarrow$ ($\Leftarrow$) refer to the electron or proton polarization parallel (anti-parallel) to the beam momentum. The transverse proton beam-spin asymmetry is

$$A_{\mathrm{UT}} = \frac{\mathrm{d}\sigma(\phi,\phi_S) - \mathrm{d}\sigma(\phi,\phi_S+\pi)}{\mathrm{d}\sigma(\phi,\phi_S) + \mathrm{d}\sigma(\phi,\phi_S+\pi)}. \tag{4}$$

The double-spin asymmetries for a longitudinally polarized electron beam are

$$A_{\mathrm{LL}} = \frac{[\mathrm{d}\sigma(\phi)^{\rightarrow\Rightarrow} + \mathrm{d}\sigma(\phi)^{\leftarrow\Leftarrow}] - [(\mathrm{d}\sigma(\phi)^{\leftarrow\Rightarrow} + \mathrm{d}\sigma(\phi)^{\rightarrow\Leftarrow}]}{\mathrm{d}\sigma(\phi)^{\rightarrow\Rightarrow} + \mathrm{d}\sigma(\phi)^{\leftarrow\Leftarrow} + (\mathrm{d}\sigma(\phi)^{\leftarrow\Rightarrow} + \mathrm{d}\sigma(\phi)^{\rightarrow\Leftarrow}]}, \tag{5}$$

$$A_{\mathrm{LT}} = \frac{[\mathrm{d}\sigma(\phi,\phi_S)^{\rightarrow} + \mathrm{d}\sigma(\phi,\phi_S+\pi)^{\leftarrow}] - [\mathrm{d}\sigma(\phi,\phi_S)^{\leftarrow} + \mathrm{d}\sigma(\phi,\phi_S+\pi)^{\rightarrow}]}{\mathrm{d}\sigma(\phi,\phi_S)^{\leftarrow} + \mathrm{d}\sigma(\phi,\phi_S)^{\rightarrow} + \mathrm{d}\sigma(\phi,\phi_S+\pi)^{\rightarrow} + \mathrm{d}\sigma(\phi,\phi_S+\pi)^{\leftarrow}}, \tag{6}$$

for longitudinally and transversely polarized proton beams, respectively. Depending on whether the electron beam helicity or proton spin is flipped, different CFF combinations enter the cross section differences. The azimuthal modulations of asymmetries, which are dominated by the interference term and thus mostly linear in the CFFs, yield [2, 9, 60–63]

$$A_{\mathrm{LU},I}^{\sin\phi} \propto \mathrm{Im}\left[F_1\mathcal{H} + \xi(F_1+F_2)\widetilde{\mathcal{H}} - \frac{t}{4m^2}F_2\mathcal{E}\right], \tag{7}$$

$$\begin{Bmatrix} A_{\mathrm{UL},I}^{\sin\phi} \\ A_{\mathrm{LL},I}^{\cos\phi} \end{Bmatrix} \propto \begin{Bmatrix} \mathrm{Im} \\ \mathrm{Re} \end{Bmatrix} \left[\xi(F_1+F_2)\left(\mathcal{H} + \frac{\xi}{1+\xi}\mathcal{E}\right) + F_1\widetilde{\mathcal{H}} - \xi\left(\frac{\xi}{1+\xi}F_1 + \frac{t}{4M^2}F_2\right)\widetilde{\mathcal{E}}\right], \tag{8}$$

$$\begin{Bmatrix} A_{\mathrm{UT},I}^{\sin(\phi-\phi_s)\cos\phi} \\ A_{\mathrm{LT},I}^{\sin(\phi-\phi_s)\sin\phi} \end{Bmatrix} \propto \begin{Bmatrix} \mathrm{Im} \\ \mathrm{Re} \end{Bmatrix} \left[\frac{t}{4M^2}\left((1-\xi)F_2\mathcal{H} - \frac{1}{1+\xi}F_1\mathcal{E}\right) - \xi^2\left(F_1 + \frac{t}{4M^2}F_2\right)\left(\mathcal{H}+\mathcal{E}\right) + \xi^2(F_1+F_2)\left(\widetilde{\mathcal{H}} + \frac{t}{4M^2}\widetilde{\mathcal{E}}\right)\right], \tag{9}$$

$$\begin{Bmatrix} A_{\mathrm{UT},I}^{\cos(\phi-\phi_s)\sin\phi} \\ A_{\mathrm{LT},I}^{\cos(\phi-\phi_s)\cos\phi} \end{Bmatrix} \propto \begin{Bmatrix} \mathrm{Im} \\ \mathrm{Re} \end{Bmatrix} \left[\frac{t}{4M^2}\left((1-\xi)F_2\widetilde{\mathcal{H}} - \frac{\xi}{1+\xi}(F_1+\xi F_2)\widetilde{\mathcal{E}} + \frac{\xi}{1+\xi}(F_1+F_2)\mathcal{E}\right) + \frac{\xi^2}{1+\xi}\left((F_1+F_2)\mathcal{H} - F_1\widetilde{\mathcal{H}}\right)\right], \tag{10}$$

where "Im" and "Re" project the imaginary and real parts of the CFFs, respectively. These relations show that different observables have different sensitivities to a given CFF. The imaginary parts of CFFs $\mathcal{H}$ and $\widetilde{\mathcal{H}}$ remarkably manifest themselves in the $\sin\phi$ modulations of single spin asymmetries A_{LU} and A_{UL}, respectively. The corresponding real parts dominate the $\cos\phi$ modulations of the unpolarized cross section of A_{LL}. The CFF $\mathcal{E}$ is most effectively accessed in transverse proton-spin asymmetries through the $\sin(\phi-\phi_s)\cos\phi$ modulation of A_{UT} and A_{LT}, whereas the $\cos(\phi-\phi_s)\cos\phi$ modulation of these asymmetries shows some sensitivity to $\widetilde{\mathcal{E}}$. Because the BH process dominates the total cross section, extracting the CFFs with high precision requires extensive measurements over a broad kinematic range, including accurate cross sections and spin asymmetries and, importantly, their azimuthal modulations.

Raw DVCS event samples at the EicC for a 3.5 GeV electron beam colliding with a 20 GeV proton beam are generated by the MC generator MILOU [64]. These are

slightly modified from the original version [65, 66], and the proton-dissociation background $ep \to e\gamma X$ is temporarily neglected. A previous study applied proper kinematic cuts to ensure DVCS dominance and removed resonance contributions by selecting events with photon-proton invariant masses above 2.0 GeV [58]. In the present analysis, realistic detector acceptance and efficiency are included, assuming a 50 mrad beam crossing angle, following the EicC Conceptual Design Report (CDR) [67]. A fast simulation framework incorporating acceptance, efficiency, and resolution is employed, which was previously established in EicC simulations of exclusive photoproduction of heavy quarkonium [29, 68, 69], exotic hadron production [70−73], the Sullivan process [74], and various inclusive processes [75]. Experimentally demanding yet essential recoil-proton detection is realized using optimized Roman pots inside the beampipe. Two accelerator operation modes are considered: high-luminosity mode $\mathcal{L} = 4\times10^{33}$ cm^{-2} s^{-1} with Roman pots optimized for the detection of particles with scattering angles larger than 10 mrad, and complementary small-angular-divergence mode, allowing detection to 5 mrad, with the luminosity reduced to 1.1×10^{33} cm^{-2} s^{-1}. Pseudo-data are generated assuming 3/4 of the running time in high-luminosity mode and 1/4 in small-angular-divergence mode (see Refs. [67, 76] for details).

The projected DVCS cross sections $\mathrm{d}\sigma(\phi)$, assuming a year of data collection, along with their statistical uncertainties are shown in Fig. 2. They are organized into 69 kinematic bins in $(x_B,\ Q^2,\ -t)$, each further subdivided into 18 ϕ-bins. Owing to the good detection efficiency, we can feasibly measure the sea quark region $0.01 < x_B < 0.1$ and safely perturbative domain $2\ \mathrm{GeV}^2 < Q^2 < 30\ \mathrm{GeV}^2$. Although the detection efficiency decreases at lower x_B, it is compensated for by the extremely high statistics achieved at $x_B \sim 0.004$ when Q^2 approaches 1 GeV^2. The detector coverage also provides welcome overlap with that of the JLab 12-GeV program in the valence region but at generally higher Q^2 values at the EicC. This safely perturbative domain without higher-twist corrections extends the high Q^2 lever arm for valence quark physics. Of particular interest is the largely unexplored domain $Q^2 \in [30.0, 80.0]$ GeV^2 with an average $-t = 0.51$ GeV^2, where sufficient statistics enable differential cross section measurements. The uncorrelated statistical uncertainties of the asymmetries in each bin are computed using a likelihood-based estimator:

$$\delta A \propto \frac{1}{f_d P_p P_e}\sqrt{\frac{1-A}{N_{\mathrm{events}}}}, \tag{11}$$

where f_d denotes the dilution factor accounting for unpolarized background contributions, and the electron and proton beam polarizations are taken as $P_e =$ 80% and $P_p =$ 70%, respectively. Here, N_{events} is the number of

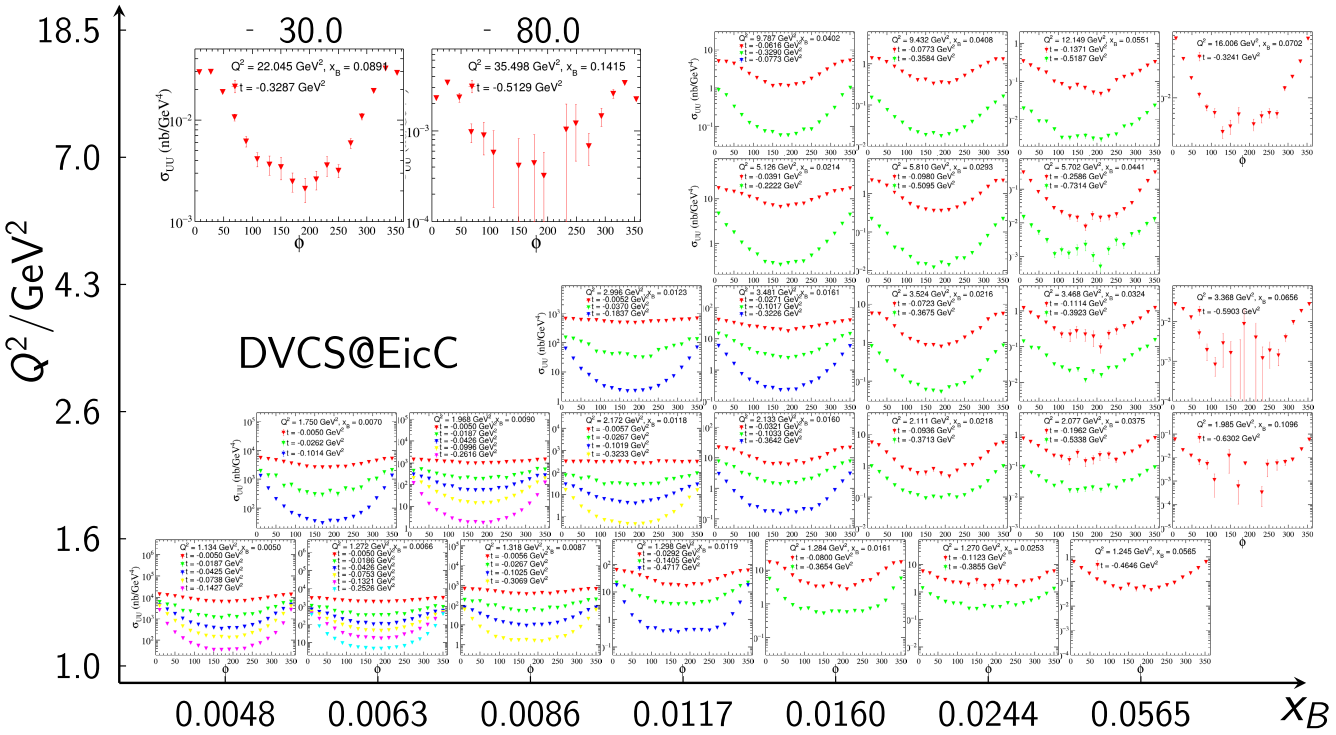

Fig. 2. (color online) Simulated four-fold unpolarized cross sections with statistical uncertainties in the bins of x_B and Q^2. In each panel, different t values in units of GeV^2 are explicitly labeled. The systematic uncertainties are not included. The central values of the pseudo-data are generated using the GK GPD model [62, 77, 78] and smeared by the statistical uncertainties.

events obtained by scaling the generated cross sections to the assumed integrated luminosity of the EicC.

The absolute statistical uncertainties of the measured asymmetries fall within approximately 1%–5% across all considered kinematic bins. The main sources of systematic uncertainty for the proposed measurement are radiative corrections and contamination from π^0 background channels. Additional contributions to systematic uncertainty include the beam-polarization uncertainties, acceptance corrections, and lepton identification. Detector optimization aims to control the total systematic uncertainty such that it remains comparable to, or smaller than, the statistical uncertainty.

Progress in global fitting techniques, particularly those representing CFFs as NNs, has made it feasible to assess the impact of the above all-asymmetry pseudo-data on CFF extraction. The connection between DVCS asymmetries and CFFs is constructed using the `Gepard` framework [32, 35, 36]. Because current world data provide essentially no constraints on the real parts of $\widetilde{\mathcal{E}}$ and $\widetilde{\mathcal{H}}$, these are assumed to vanish in our analysis (following Ref. [36]). The NN architecture shown in Fig. 3 is implemented using the `PyTorch` machine-learning library, with the hyperparameters chosen for optimal extrapolation into unmeasured kinematic regimes. To ensure the complete independence of the real and imaginary parts of CFFs, a modular NN composed of independent sub-networks is constructed. The activation function for neurons in the hidden layers is

$$f(x) = \begin{cases} 0 & \text{for } x < 0, \\ \mathrm{e}^x - 1 & \text{for } x > 0, \end{cases} \tag{12}$$

which provides the necessary non-linearity. Training is performed via a back-propagation algorithm using the Adam (adaptive moment estimation) optimizer [79], minimizing the uncertainty-weighted Huber loss function [80−84]. The training data in the valence region include measurements from the JLab collaborations [63, 85−89], COMPASS [90], and HERMES [91], whereas the small-x_B region ($10^{-4} \lesssim x_B \lesssim 10^{-3}$) is constrained by ZEUS and H1 data [92−94]. All datasets are truncated with the kinematic cuts $Q^2 > 1.5\,\mathrm{GeV}^2, -t/Q^2 < 0.2$ to suppress the higher-twist contribution. The combined world dataset is randomly split into a 90% training set and 10% test set and data leakage and overfitting are controlled using the standard early-stopping technique. Linearization and normalization of the input variables enable fast, high precision convergence, facilitating practical generation of a large number of MC replica datasets via bootstrapping to propagate statistical uncertainties from the data to the extracted CFFs. The network depth and width and the choice of loss function are optimized based on fitting and validation performance.

The actual χ^2 per data point is in the range 1.0 ~ 2.0 for each dataset (see Table 1). The skewness ξ-dependence of the CFFs extracted from existing world data at $Q^2 = 4.0$ GeV^2 and $-t = 0.4$ GeV^2 is shown by the blue band in Fig. 4. Similarly, the $-t$ dependence at $Q^2 = 4.0$ GeV^2 and $\xi = 0.01$ GeV^2 is illustrated in Fig. 5, whereas the Q^2 dependence at $\xi = 0.01$ and $-t = 0.4$ GeV^2 is displayed in Fig. 6. The results in the valence region agree with the conclusions of previous analyses. The extrapolation behavior is consistent with that obtained using *PARTONS* [33]; however, our uncertainties are relatively smaller, likely owing to the assumption of the vanishing real part of $\widetilde{\mathcal{E}}$ and $\widetilde{\mathcal{H}}$.

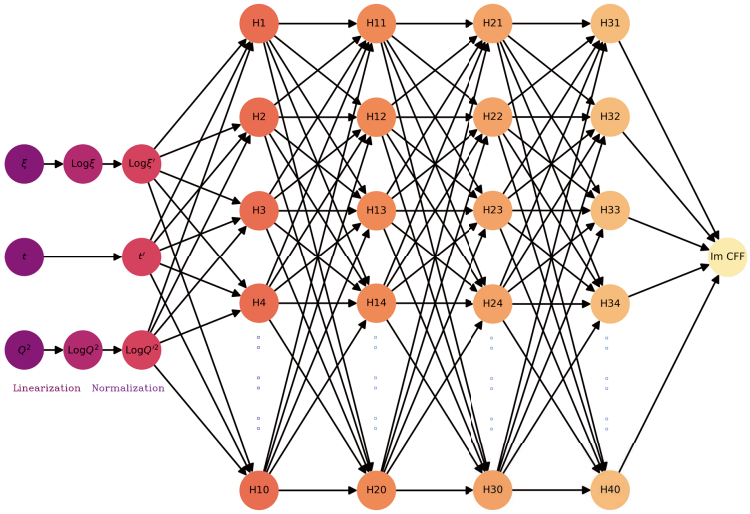

Fig. 3. (color online) Single neural network parameterizes the imaginary part of one of the CFFs, and a similar net represents the real part. The input values (ξ, t, Q^2) after linearization and normalization are fed into three input neurons and then propagated through four hidden layers with ninety neurons each. Therefore, the architecture is ($3 \to 90 \to 90 \to 90 \to 90 \to 1$).

Table 1. Fitted χ^2 per data point before and after including the EicC pseudo-data for asymmetries.

Observable	Collaboration	Ref.	χ^2	$\chi^2_{\mathrm{w/EicC}}$
A_{LU}	CLAS	[95]	1.30	1.47
A_{LU}	HERMES	[96]	0.95	0.81
A_{UT}	HERMES	[97]	1.50	1.01
A_{LL}	CLAS	[95]	2.09	2.12
A_{UL}	CLAS	[95]	3.54	1.13
σ_{UU}	H1	[98]	0.69	0.63
σ_{UU}	H1	[99]	0.90	0.64
σ_{UU}	ZEUS	[100]	0.98	1.05
A_{LU}	CLAS	[101]	0.43	0.42
A_{LU}	HALL A	[102]	1.05	1.14
σ_{UU}	CLAS	[101]	0.95	0.88
σ_{UU}	HALL A	[102]	1.64	1.80
σ_{UU}	HALL A	[85]	1.21	0.90
Total			1.1	0.9

The central values of the CFFs and the predicted cross sections and asymmetries beyond the valence region are approximately zero within large uncertainties, reflecting the marginal impact of current data in the sea-quark and gluon domains. Therefore, the pseudo-data for unpolarized cross sections are not included in the present impact study because their relative statistical uncertainties are inversely proportional to N_{events}. Consequently, a substantial reduction in the uncertainty of Re$\mathcal{H}$ should not be expected after including the EicC pseudo-data, as suggested by Eq. (2). Within the NN framework, the predicted asymmetry magnitudes are smeared by randomly resampling the central values according to the generated statistical uncertainties of Eq. (11). The networks are then retrained on the full set of measured and simulated experimental data to assess the genuine impact of the EicC machine. Although realistic systematic uncertainties would enlarge the final error bands, the global analysis clearly demonstrates that the EicC can prominently improve the precision of all relevant CFFs to $\xi \sim 10^{-4}$. In particular, the uncertainties of CFFs in the sea-quark region are sig-

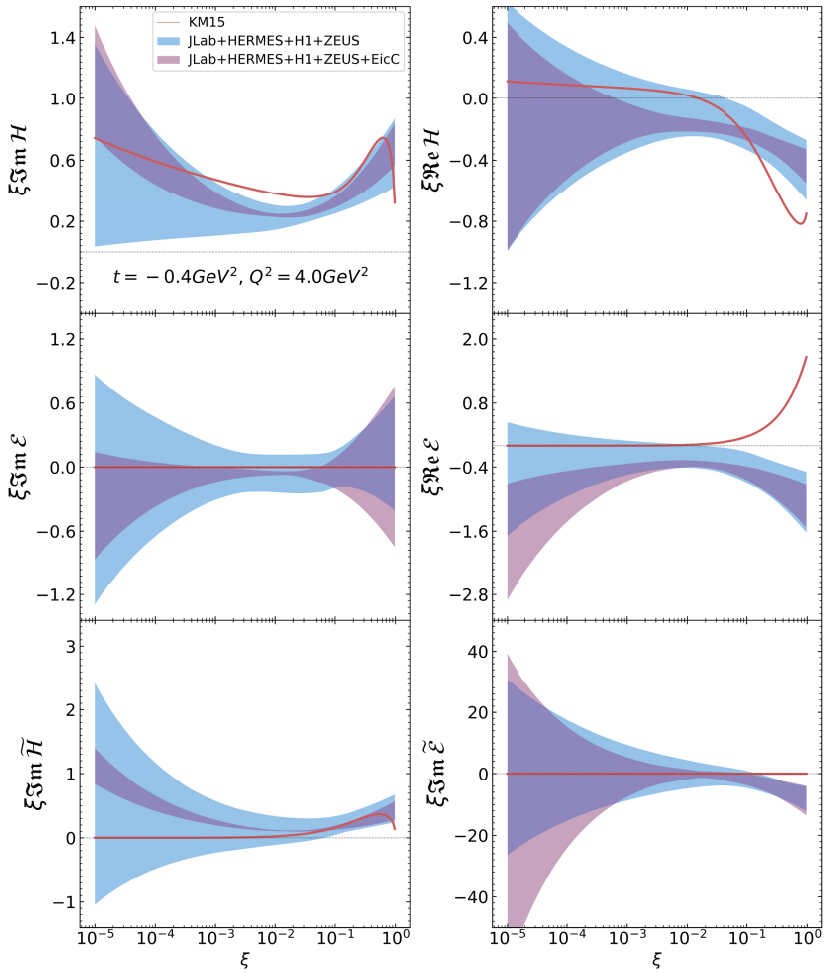

Fig. 4. (color online) Extraction of CFFs versus skewness ξ at $Q^2 = 4.0$ GeV^2 and $-t = 0.4$ GeV^2. The blue and red error bands are uncertainties before and after including the pseudodata of asymmetries at the EicC, respectively.

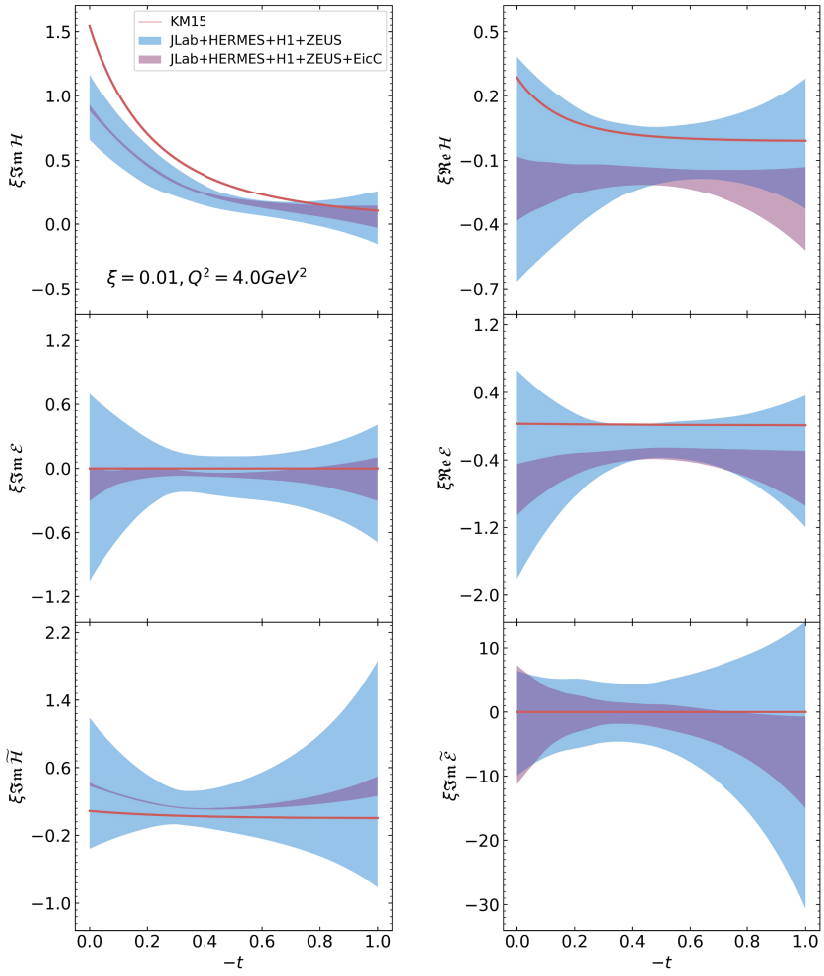

Fig. 5. (color online) Extraction of CFFs versus $-t$ at $Q^2 = 4.0$ GeV^2 and $\xi = 0.01$ GeV^2.

nificantly reduced, as indicated by the light-red bands in Fig. 4. The $-t$ dependence of CFFs in the sea regime is also extracted with good precision up to 1.0 GeV^2 (Fig. 5). Thus, the EicC will provide an accurate spatial tomography of the sea quarks inside the nucleon through Fourier transform, albeit by relying on assumptions or models to extrapolate beyond the experimentally accessible kinematic region. Likewise, the influence of EicC data on the Q^2 dependence of CFFs is evident up to 20 GeV^2 in the sea domain (Fig. 6), revealing the possibility of GPD deconvolution from DVCS data via QCD scale evolution across a broad Q^2 range.

On the methodological side, the EicC pseudo-data provide important validation of the extraction strategy over a wide kinematic range. As expected, the error bands of CFFs obtained after including the EicC pseudo-data remain consistent with those derived solely from existing measurements, serving as a non-trivial closure test of the NN procedure. However, noticeable deviations exceeding 1σ appear in the leading CFFs Re$\mathcal{H}$ and Re$\mathcal{E}$ in certain regions, reflecting the strong clustering of current data in a limited portion of phase space. With further experimental input, improved lattice-QCD constraints, and refined theoretical guidance, NN methods offer a promising solution to balancing bias minimization and flexibility of the model.

III. SUMMARY AND CONCLUSION

The EicC is designed to probe the sea-quark region, providing kinematic coverage between JLab and the EIC at the BNL. The DVCS data of unprecedented accuracy at the EicC are expected to considerably improve our understanding of proton tomography in terms of the GPD. A previous Bayesian reweighting study [58] showed that even a single day of data collection with a transversely polarized proton beam at the EicC would surpass the constraining power of existing HERMES fixed-target measurements in the sea-quark regime [97].

NN parameterizations of CFFs enable a precise extraction and disentanglement of the CFFs with a true global fit over all observables. In this study, we construct a flexible NN architecture to simultaneously extract the CFFs from existing data and assess the constraining

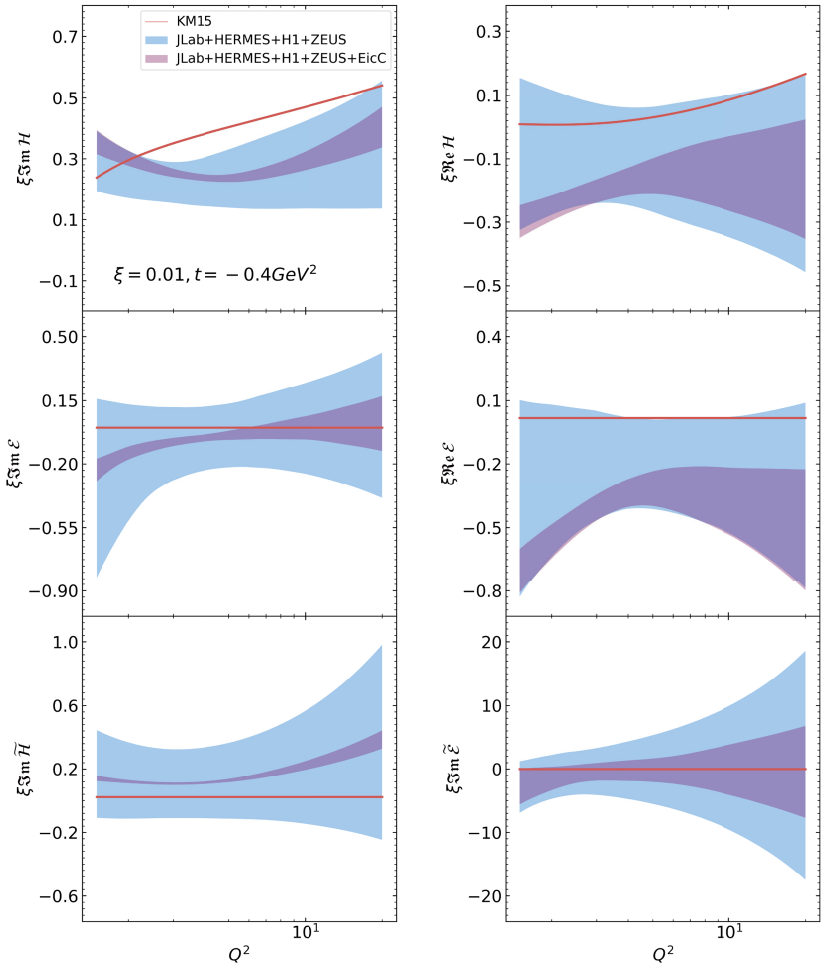

Fig. 6. (color online) Extraction of CFFs versus Q^2 at $\xi = 0.01$ and $-t = 0.4$ GeV^2.

power of future EicC asymmetry measurements. A significant reduction in the uncertainties of all relevant CFFs is observed when including the projected EicC data. This also constitutes a valuable closure test of the NN methodology, suggesting the need for additional theoretical input to further stabilize extrapolations. The framework is readily extendable to incorporate forthcoming datasets, including those expected from JLab [103] and the EIC [15, 104]. Higher-twist contributions can feasibly be incorporated into our global fit in the near future [105]. Only then would the importance of the extension to high Q^2 domain become clear for valence quark physics through a more direct comparison between the EicC and JLab.

This study represents a step toward the reliable extraction of GPDs at leading order by means of flexible GPD parameterizations in the same manner as PDFs being extracted from multi-dimensional structure functions. However, achieving global fits using next-to-leading [105–106] and next-to-next-to-leading order [107−110] frameworks remains a major challenge [47].

ACKNOWLEDGMENTS

We are grateful to Aiqiang Guo, Yu-Tie Liang, and Weizhi Xiong for providing the fast simulation of the EicC detector. We gratefully acknowledge the support of the High Performance Computing Cluster of the Southern Nuclear Science Computing Center (SNSC).

References

[1] M. Diehl, Phys. Rept. **388**, 41 (2003), arXiv: hep-ph/0307382
[2] A. V. Belitsky and A. V. Radyushkin, Phys. Rept. **418**, 1 (2005), arXiv: hep-ph/0504030
[3] M. Guidal, H. Moutarde, and M. Vanderhaeghen, Rept. Prog. Phys. **76**, 066202 (2013), arXiv: 1303.6600
[4] S. Diehl, Prog. Part. Nucl. Phys. **133**, 104069 (2023)
[5] D. Müller, D. Robaschik, B. Geyer *et al.*, Fortsch. Phys.

42, 101 (1994), arXiv: hep-ph/9812448
[6] X. D. Ji, Phys. Rev. D **55**, 7114 (1997), arXiv: hep-ph/9609381
[7] X. D. Ji, Phys. Rev. Lett. **78**, 610 (1997), arXiv: hep-ph/9603249
[8] A. V. Radyushkin, Phys. Rev. D **56**, 5524 (1997), arXiv: hep-ph/9704207
[9] M. Diehl and S. Sapeta, Eur. Phys. J. C **41**, 515 (2005), arXiv: hep-ph/0503023
[10] A. Accardi *et al*., Eur. Phys. J. A **52**, 268 (2016), arXiv: 1212.1701
[11] R. A. Khalek *et al*., Nucl. Phys. A **1026**, 122447 (2022), arXiv: 2103.05419
[12] A. Accardi *et al*., Eur. Phys. J. A **60**, 173 (2024), arXiv: 2306.09360
[13] X. Cao, L. Chang, N. Chang *et al*., Nucl. Tech. **43**, 020001 (2020)
[14] X. Cao, X. Chen, C. Gong *et al*., Sci. Sin. Phys. Mech. Astro. **50**, 112005 (2020)
[15] D. P. Anderle *et al*., Front. Phys. (Beijing) **16**, 64701 (2021), arXiv: 2102.09222
[16] J. L. Abelleira Fernandez *et al*. (LHeC Study Group), J. Phys. G **39**, 075001 (2012), arXiv: 1206.2913
[17] P. Agostini *et al*. (LHeC, FCC-he Study Group), J. Phys. G **48**, 110501 (2021), arXiv: 2007.14491
[18] J. P. Ralston and B. Pire, Phys. Rev. D **66**, 111501 (2002), arXiv: hep-ph/0110075
[19] M. Diehl, Eur. Phys. J. C **25**, 223 (2002) [Erratum: Eur. Phys. J. C **31**, 277 (2003)], arXiv: hep-ph/0205208
[20] M. Burkardt, Phys. Rev. D **62**, 071503 (2000) [Erratum: Phys. Rev. D **66**, 119903 (2002)], arXiv: hep-ph/0005108
[21] M. Burkardt, Int. J. Mod. Phys. A **18**, 173 (2003), arXiv: hep-ph/0207047
[22] M. V. Polyakov, Phys. Lett. B **555**, 57 (2003), arXiv: hep-ph/0210165
[23] V. Bertone, H. Dutrieux, C. Mezrag *et al*., Phys. Rev. D **103**, 114019 (2021), arXiv: 2104.03836
[24] E. Moffat, A. Freese, I. Cloët *et al*., Phys. Rev. D **108**, 036027 (2023), arXiv: 2303.12006
[25] H. Moutarde, Phys. Rev. D **79**, 094021 (2009), arXiv: 0904.1648
[26] M. Boër and M. Guidal, J. Phys. G **42**, 034023 (2015), arXiv: 1412.4651
[27] K. Kumerički, D. Müller, and M. Murray, Phys. Part. Nucl. **45**, 723 (2014), arXiv: 1301.1230
[28] S. Forte, L. Garrido, J. I. Latorre *et al*., JHEP **05**, 062 (2002), arXiv: hep-ph/0204232
[29] X. Wang, X. Cao, Y. Lu *et al*., (2025), arXiv: 2509.14549
[30] Z. Ye, J. Arrington, R. J. Hill *et al*., Phys. Lett. B **777**, 8 (2018), arXiv: 1707.09063
[31] L. Kotz, A. Courtoy, P. Nadolsky *et al*., Phys. Rev. D **109**, 074027 (2024), arXiv: 2311.08447
[32] K. Kumericki, D. Mueller, and A. Schafer, JHEP **07**, 073 (2011), arXiv: 1106.2808
[33] H. Moutarde, P. Sznajder, and J. Wagner, Eur. Phys. J. C **79**, 614 (2019), arXiv: 1905.02089
[34] L. Calero Diaz and D. Keller, Phys. Rev. D **112**, 096001 (2025), arXiv: 2509.18331
[35] K. Kumerički, Nature **570**, E1 (2019)
[36] M. Čuić, K. Kumerički, and A. Schäfer, Phys. Rev. Lett. **125**, 232005 (2020), arXiv: 2007.00029
[37] A. Hobart *et al*. (CLAS Collaboration), Phys. Rev. Lett. **133**, 211903 (2024), arXiv: 2406.15539
[38] I. V. Musatov and A. V. Radyushkin, Phys. Rev. D **61**, 074027 (2000), arXiv: hep-ph/9905376
[39] D. Mueller and A. Schafer, Nucl. Phys. B **739**, 1 (2006), arXiv: hep-ph/0509204
[40] K. A. Mamo and I. Zahed, Phys. Rev. Lett. **133**, 241901 (2024), arXiv: 2411.04162
[41] S. Xu *et al*. (BLFQ), Phys. Rev. D **104**, 094036 (2021), arXiv: 2108.03909
[42] H. Dutrieux, H. Dutrieux, O. Grocholski *et al*., Eur. Phys. J. C **82**, 252(2022) [Erratum: Eur. Phys. J. C **82**, 389 (2022)], arXiv: 2112.10528
[43] A. Dotson *et al*., (2025), arXiv: 2504.13289
[44] K. Kumericki, D. Mueller, and K. Passek-Kumericki, Nucl. Phys. B **794**, 244 (2008), arXiv: hepph/0703179
[45] K. Kumerički and D. Mueller, Nucl. Phys. B **841**, 1 (2010), arXiv: 0904.0458
[46] H. Moutarde, P. Sznajder, and J. Wagner, Eur. Phys. J. C **78**, 890 (2018), arXiv: 1807.07620
[47] M. Čuić, G. Duplančić, K. Kumerički *et al*., JHEP **12**, 192 (2023) [Erratum: JHEP **02**, 225 (2024)], arXiv: 2310.13837
[48] Y. Guo, X. Ji, M. G. Santiago *et al*., JHEP **05**, 150 (2023), arXiv: 2302.07279
[49] Y. Guo, F. P. Aslan, X. Ji *et al*., (2025), arXiv: 2509.08037
[50] M. Constantinou *et al*., Prog. Part. Nucl. Phys. **121**, 103908 (2021), arXiv: 2006.08636
[51] H. W. Lin, Phys. Rev. Lett. **127**, 182001 (2021), arXiv: 2008.12474
[52] J. Holligan and H. W. Lin, Phys. Rev. D **110**, 034503 (2024), arXiv: 2312.10829
[53] S. Bhattacharya, K. Cichy, M. Constantinou *et al*., Phys. Rev. D **110**, 054502 (2024), arXiv: 2405.04414
[54] M. J. Riberdy, H. Dutrieux, C. Mezrag *et al*., Eur. Phys. J. C **84**, 201 (2024), arXiv: 2306.01647
[55] X. Ji, Phys. Rev. Lett. **110**, 262002 (2013), arXiv: 1305.1539
[56] X. Ji, Sci. China Phys. Mech. Astron. **57**, 1407 (2014), arXiv: 1404.6680
[57] A. V. Radyushkin, Phys. Rev. D **96**, 034025 (2017), arXiv: 1705.01488
[58] X. Cao and J. Zhang, Eur. Phys. J. C **83**, 505 (2023), arXiv: 2301.06940
[59] A. Bacchetta, U. D'Alesio, M. Diehl *et al*., Phys. Rev. D **70**, 117504 (2004), arXiv: hep-ph/0410050
[60] A. V. Belitsky, D. Mueller, and A. Kirchner, Nucl. Phys. B **629**, 323 (2002), arXiv: hep-ph/0112108
[61] A. V. Belitsky and D. Mueller, Phys. Rev. D **82**, 074010 (2010), arXiv: 1005.5209
[62] P. Kroll, H. Moutarde, and F. Sabatie, Eur. Phys. J. C **73**, 2278 (2013), arXiv: 1210.6975
[63] N. d'Hose, S. Niccolai, and A. Rostomyan, Eur. Phys. J. A **52**, 151 (2016)
[64] E. Perez, L. Schoeffel, and L. Favart, (2004), arXiv: hep-ph/0411389
[65] E. C. Aschenauer, S. Fazio, K. Kumericki *et al*., JHEP **09**, 093 (2013), arXiv: 1304.0077
[66] E. C. Aschenauer, S. Fazio, J. H. Lee *et al*., Rept. Prog. Phys. **82**, 024301 (2019), arXiv: 1708.01527
[67] C. B. e. a. Luis Albino, Daniele P. Anderle (2025), EicC Conceptual Design Report Volume II - Physics & Detector, to appear.
[68] X. Wang, X. Cao, A. Guo *et al*., Eur. Phys. J. C **84**, 684

(2024), arXiv: 2311.07008
[69] X. Cao, F. K. Guo, Y. T. Liang *et al.*, Phys. Rev. D **101**, 074010 (2020), arXiv: 1912.12054
[70] X. Cao, Front. Phys. (Beijing) **18**, 44600 (2023), arXiv: 2301.11253
[71] X. Cao, J. P. Dai, and Z. Yang, Eur. Phys. J. C **81**, 184 (2021), arXiv: 2011.09244
[72] Z. Yang, X. Cao, Y. T. Liang *et al.*, Chin. Phys. C **44**, 084102 (2020), arXiv: 2003.06774
[73] X. Cao and J. p. Dai, Phys. Rev. D **100**, 054033 (2019), arXiv: 1904.06015
[74] Z. Lu, Z. Yu, T. Lin *et al.*, (2025), arXiv: 2512.01720
[75] C. Zeng, T. Liu, P. Sun *et al.*, Phys. Rev. D **106**, 094039 (2022), arXiv: 2208.14620
[76] R. He *et al.*, Nucl. Sci. Tech. **34**, 205 (2023)
[77] S. V. Goloskokov and P. Kroll, Eur. Phys. J. C **65**, 137 (2010), arXiv: 0906.0460
[78] S. V. Goloskokov and P. Kroll, Eur. Phys. J. A **47**, 112 (2011), arXiv: 1106.4897
[79] D. P. Kingma and J. Ba, (2014), arXiv: 1412.6980
[80] J. Grigsby, B. Kriesten, J. Hoskins *et al.*, Phys. Rev. D **104**, 016001 (2021), arXiv: 2012.04801
[81] M. Almaeen, T. Alghamdi, B. Kriesten *et al.*, Eur. Phys. J. C **85**, 499 (2025), arXiv: 2405.05826
[82] M. Almaeen, J. Grigsby, J. Hoskins *et al.*, (2022), arXiv: 2207.10766
[83] D. Q. Adams *et al.*, (2024), arXiv: 2410.23469
[84] F. Hossen *et al.*, (2024), arXiv: 2408.11681
[85] M. Defurne *et al.*, Nature Commun. **8**, 1408 (2017), arXiv: 1703.09442
[86] C. E. Hyde, M. Guidal, and A. V. Radyushkin, J. Phys. Conf. Ser. **299**, 012006 (2011), arXiv: 1101.2482
[87] V. Burkert *et al.* (CLAS Collaboration), Eur. Phys. J. A **57**, 186 (2021), arXiv: 2103.12651
[88] S. Fucini, M. Hattawy, M. Rinaldi *et al.*, Eur. Phys. J. A **57**, 273 (2021), arXiv: 2105.00435
[89] A. Afanasev *et al.*, Eur. Phys. J. A **57**, 300 (2021), arXiv: 2105.06540
[90] R. Akhunzyanov *et al.* (COMPASS Collaboration), Phys. Lett. B **793**, 188 (2019) [Erratum: Phys. Lett. B **800**, 135129 (2020)], arXiv: 1802.02739
[91] A. Airapetian *et al.* (HERMES Collaboration), JHEP **10**, 042 (2012), arXiv: 1206.5683
[92] S. Chekanov *et al.* (ZEUS Collaboration), Phys. Lett. B **573**, 46 (2003), arXiv: hep-ex/0305028
[93] C. Adloff *et al.* (H1 Collaboration), Phys. Lett. B **517**, 47 (2001), arXiv: hep-ex/0107005
[94] F. D. Aaron *et al.* (H1 Collaboration), Phys. Lett. B **681**, 391 (2009), arXiv: 0907.5289
[95] S. Pisano *et al.* (CLAS Collaboration), Phys. Rev. D **91**, 052014 (2015), arXiv: 1501.07052
[96] A. Airapetian *et al.* (HERMES Collaboration), JHEP **07**, 032 (2012), arXiv: 1203.6287
[97] A. Airapetian *et al.* (HERMES Collaboration), JHEP **06**, 066 (2008), arXiv: 0802.2499
[98] F. D. Aaron *et al.* (H1 Collaboration), Phys. Lett. B **659**, 796 (2008), arXiv: 0709.4114
[99] A. Aktas *et al.* (H1 Collaboration), Eur. Phys. J. C **44**, 1 (2005), arXiv: hep-ex/0505061
[100] S. Chekanov *et al.* (ZEUS Collaboration), JHEP **05**, 108 (2009), arXiv: 0812.2517
[101] H. S. Jo *et al.* (CLAS Collaboration), Phys. Rev. Lett. **115**, 212003 (2015), arXiv: 1504.02009
[102] M. Defurne *et al.* (Jefferson Lab Hall A), Phys. Rev. C **92**, 055202 (2015), arXiv: 1504.05453
[103] J. Arrington *et al.* (Jefferson Lab SoLID), J. Phys. G **50**, 110501 (2023), arXiv: 2209.13357
[104] E. C. Aschenauer *et al.*, Phys. Rev. D **112**, 036010 (2025), arXiv: 2503.05908
[105] V. M. Braun, Y. Ji, and A. N. Manashov, Phys. Rev. D **111**, 076011 (2025), arXiv: 2501.08185
[106] V. M. Braun, Y. Ji, and A. N. Manashov, JHEP **01**, 078 (2023), arXiv: 2211.04902
[107] V. M. Braun, A. N. Manashov, S. Moch *et al.*, JHEP **09**, 117 (2020) [Erratum: JHEP **02**, 115 (2022)], arXiv: 2007.06348
[108] V. M. Braun, A. N. Manashov, S. Moch *et al.*, Phys. Rev. D **104**, 094007 (2021), arXiv: 2106.01437
[109] V. M. Braun, Y. Ji, and J. Schoenleber, Phys. Rev. Lett. **129**, 172001 (2022), arXiv: 2207.06818
[110] Y. Ji and J. Schoenleber, JHEP **01**, 053 (2024), arXiv: 2310.05724